Size distributions of ionic aerosols measured at Waliguan Observatory: Implication for nitrate gas-to-particle transfer processes in the free troposphere

Jianzhong Ma and Jie Tang
Chinese Academy of Meteorological Sciences, Beijing, People's Republic of China

Shao-Meng Li
Atmospheric Environment Service, Ontario, Canada

Mark Z. Jacobson
Department of Civil and Environmental Engineering, Stanford University, California, USA

Received 26 December 2002; revised 7 May 2003; accepted 15 May 2003; published 9 September 2003.

[1] Waliguan Observatory (WO) is a land-based Global Atmosphere Watch baseline station on the Tibetan Plateau. Size-resolved ionic aerosols (NH_4^+, Na^+, K^+, Ca^{2+}, Mg^{2+}, SO_4^{2-}, Cl^-, NO_3^- CO_3^{2-}, formate, acetate and oxalate), organic aerosols, black carbon and gaseous HNO_3 and SO_2 were measured during an intensive fall-winter field experiment. The observational data were analyzed with a focus on the partitioning of nitrate between the gas and particle phases. Nitrate was found to exist mainly in the particle phase with a typical particulate-to-total nitrate ratio, i.e., $NO_3^-(p)/(NO_3^-(p) + HNO_3(g))$, of about 0.9. It was also found that the size distribution pattern of particulate nitrate at WO varied in different samples and the amount of particulate nitrate residing in the fine mode ($D_p < 2.0$ μm) was typically larger than or comparable with that in the coarse mode. A gas-particle chemical equilibrium model was used to predict these particulate nitrate size distributions. The size distributions of particulate nitrate were reasonably reproduced with the model within the uncertainties caused by the detection limits. The chemical pathways for the formation of particulate nitrate at WO were analyzed with the size distributions of measured ionic aerosols. It was demonstrated that fine nitrate particles may have been produced by the reaction of gaseous nitric acid with gaseous ammonia, while coarse nitrate particles may have been generated via the condensation of nitric acid on the surface of mineral aerosols. The signature of biomass burning at WO was found to be associated with black carbon as well as the accumulation of potassium and oxalate in the fine particles. *INDEX TERMS:* 0305 Atmospheric Composition and Structure: Aerosols and particles (0345, 4801); 0365 Atmospheric Composition and Structure: Troposphere—composition and chemistry; 0322 Atmospheric Composition and Structure: Constituent sources and sinks; *KEYWORDS:* particulate nitrate, nitric acid, gas-particle conversion, model, free troposphere

Citation: Ma, J., J. Tang, S.-M. Li, and M. Z. Jacobson, Size distributions of ionic aerosols measured at Waliguan Observatory: Implication for nitrate gas-to-particle transfer processes in the free troposphere, *J. Geophys. Res.*, *108*(D17), 4541, doi:10.1029/2002JD003356, 2003.

1. Introduction

[2] The partitioning of nitrate between the gas and particle phases is an important process that has a significant influence on tropospheric chemistry and the biogeochemical cycling of nitrogen compounds. Nitric acid (HNO_3) can react with ammonia (NH_3) to produce fine ammonium nitrate particles [e.g., *Stelson et al.*, 1979; *Stelson and Seinfeld*, 1982; *Moya et al.*, 2001; *Lefer and Talbot*, 2001]. Mineral and biomass burning aerosols can affect the HNO_3 gas phase abundance in the troposphere by providing a chemical sink for HNO_3 [*Song and Carmichael*, 2001a; *Tabazadeh et al.*, 1998]. The scavenging of HNO_3 can also take place in sea-salt aerosols, leading to the formation of coarse nitrate particles [*Savoie and Prospero*, 1982; *Gard et al.*, 1998]. The formation of particulate nitrate may also occur through nighttime heterogeneous reactions of gaseous NO_3 and N_2O_5 on the wet surface of sulfate particles among others [*Ehhalt and Drummond*, 1982; *Dentener and Crutzen*, 1993; *Dentener et al.*, 1996].

[3] Both natural and anthropogenic aerosols are believed to be transported over long distances. The conti-

0148-0227/03/2002JD003356$09.00

nental sulfate and nitrate have been found in the background atmosphere over the Pacific Ocean [*Prospero and Savoie*, 1989; *Savoie and Prospero*, 1989]. Particles consisting of sulfates, nitrate, organics, black carbon and fly ash, among several other pollutants, were recently observed over the tropical Indian Ocean [*Lelieveld et al.*, 2001]. During long-range transport, primary particles from different sources can interact with secondary gaseous precursors (e.g., SO_2, H_2SO_4, NH_3, N_2O_5 and HNO_3) [*Dentener et al.*, 1996; *Song and Carmichael*, 1999, 2001b]. Therefore the chemical composition and size distribution of particles may vary significantly from the near-source area to the receptor region due to the interactions.

[4] HNO_3 tends to be preferentially present in the particle phase at urban and pollution-impacted locations, because of higher gaseous NH_3 mixing ratio and higher mineral aerosol loadings due to wind blown soils and road construction debris [*Song and Carmichael*, 2001b]. The observed average ratios of particulate nitrate to total nitrate are larger than 0.8 at urban and pollution-impacted locations, but only ~0.3 at remote sites and free troposphere over the Pacific [*Song and Carmichael*, 2001a, and references therein]. A spring maximum in particulate nitrate concentrations associated with long-range transport of alkaline components (Ca^{2+} and K^+) were found at Cheju Island, Korea [*Carmichael et al.*, 1997; *Chen et al.*, 1997] and Mauna Loa Observatory, Hawaii [*Perry et al.*, 1999]. The nitrate size-distribution measured at Cheju Island, Korea shows a prominent primary peak in the calcium-rich coarse mode [*Carmichael et al.*, 1996]. The nitrate size-distribution measured during the First Aerosol Characterization Experiment (ACE 1) tends to be shifted to the coarse mode, corresponding to the sodium size-distribution in the remote marine boundary [e.g., *Fridlind and Jacobson*, 2001].

[5] The Waliguan Observatory (WO) is a land-based Global Atmosphere Watch (GAW) baseline station, located at the northeastern part of the Tibetan Plateau (36°17′N, 100°54′E, 3816 m a.s.l.). The observational data at this site provide valuable insights into chemical characteristics of particles in the middle troposphere over the remote continental region. It has been shown that particles at WO are predominantly from natural sources, mainly from soil and crust [*Wen et al.*, 2001; *Gao and Anderson*, 2001], but the perturbations from human sources also exist as indicated by black carbon concentrations at this site [*Tang et al.*, 1999]. A special study on aerosol chemical size distribution was carried out at WO during the fall-winter period [*Li et al.*, 2000]. The results indicate relatively high levels of three components, water-soluble organic carbon (WSOC), Ca^{2+} + CO_3^{2-}, and NH_4^+ + SO_4^{2-}, with a dominant accumulation mode for WSOC, NH_4^+ and SO_4^{2-} and a prominent coarse mode for Ca^{2+} and CO_3^{2-}.

[6] In this paper, the size distributions of ionic aerosols and gaseous nitric acid measured at WO are presented. The predicted size distributions of particulate nitrate with a gas-particle chemical equilibrium model are also shown in comparison with the measurements. Our purpose is to investigate the nitrate equilibration status between the gas and particle phases at WO and its implication for nitrate gas-to-particle transfer processes in the free troposphere.

2. Methods

2.1. Site Description

[7] The Waliguan Observatory (WO) is located at the top of a mountain, Mt. Waliguan, in Qinghai Province of China. Figure 1 shows the surrounding topography within 100 km distance from Mt. Waliguan. Mt. Waliguan is an isolated peak with an elevation of about 600 m relative to the surrounding landmass. Xining City, the capital of Qinghai Province, is located about 90 km to the northeast of Mt. Waliguan. There are several high mountains (~4000 m a.s.l.) between Xining and Mt. Waliguan. A town with a population of 30,000 and light industry is located 30 km to the west of Mt. Waliguan. The WO site is relatively isolated from industry, forest, and population centers. It is relatively dry, windy and receives little precipitation with a typical continental plateau climate. Air masses at WO are usually affected by upslope flow, which brings in air from the boundary layer during the day, while at night WO is affected by downslope flow, which brings in air from the free troposphere. The routine measurement program at WO covers most baseline measurements with an emphasis on greenhouse gases and atmospheric ozone [*Tang et al.*, 1995]. Additional measurements of trace gases and aerosols are made occasionally for some periods for special research [e.g., *Ma et al.*, 2002; *Li et al.*, 2000].

2.2. Experimental

[8] The data on the chemical size distribution of aerosols at WO were obtained through a special study as reported by *Li et al.* [2000]. The experiment was carried out during the fall-winter periods, specifically in October–November 1997 and January 1998. There were 20 samples obtained in total, half for the first period, and half for the second period. A Micro Orifice Uniform Deposit Impactor (MOUDI) [*Marple et al.*, 1991] was used with Teflon filters on 11 impact stages and a back filter stage. The respective 50% cut-off sizes were 0.032, 0.056, 0.093, 0.17, 0.305, 0.55, 1, 1.8, 3.1, 6.2, 9.9 and 18 μm of particle aerodynamic diameter. The MOUDI was deployed at 3 meters above the ground at the highest point of the station with a domed cover about 30 cm above the inlet. The sampled air was not purposely dried, since relative humidity at WO is quite low, generally about 20–30% for clear days, in autumn and winter. The nighttime air mass at WO is observed to typically have free tropospheric characteristics. Hence each sampling period lasted for 12 hours at night, from 7 p.m. to 7 a.m. local time. Samples and blanks were shipped to the laboratories in Beijing and Toronto. They were extracted in low-carbonate (<10 ppb) deionized water in borosilicate vials and analyzed for inorganic and organic ions using ion chromatography. The detection limits were estimated to be 0.04(NH_4^+), 0.01(Na^+), 0.01(K^+), 0.20(Ca^{2+}), 0.02(Mg^{2+}), 0.06(SO_4^{2-}), 0.07(Cl^-) and 0.09(NO_3^-) μg m^{-3}(air). Half of the samples and blanks were also analyzed for carbonate and water-soluble organic carbon (WSOC) using a Shimadzu 5000A TOC analyzer. The TOC method involves acid titration of the extract solution to volatilize carbonate into CO_2, that is then measured using a non-dispersive

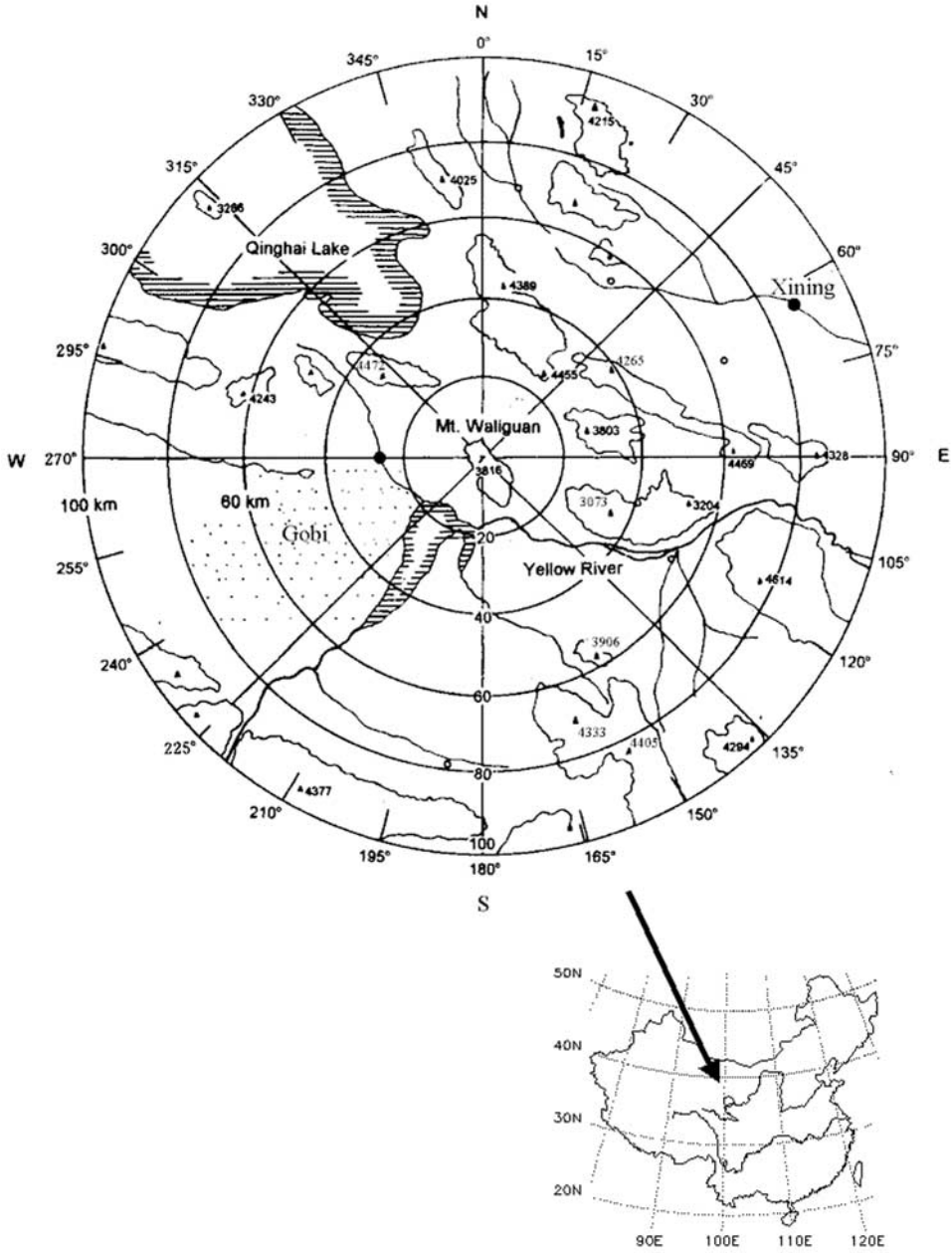

Figure 1. Surrounding topography within 100 km distance from Mt. Waliguan. Smaller map at the right-bottom shows its position in China.

infrared (NDIR) detector. WSOC is determined by injecting the sample extract into a combustion chamber by a Pt catalyst maintained at 680°C. The combusted sample is then delivered to the same NDIR detector for measurement. The method is similar to that used by *Sempere and Kawamura* [1996].

[9] Addition data on black carbon and gaseous HNO_3 and SO_2 observed at WO were used in this study [*Tang et al.*, 1999; *Ma et al.*, 2002, and reference therein]. Black carbon concentrations are routinely measured at WO using an Aethalometer, AE-10 of the Magee Scientific Co, USA. The working principal of the instrument is based on strong optical absorption by black carbon aerosols for visible light [*Hansen et al.*, 1984]. Quartz-fibroid films were used as filters, which could eliminate the effect of non-absorptive components on the measurements of transparency [*Rosen et al.*, 1978]. The instrument was placed in the laboratory of WO, being connected outside by an aluminum tube with a diameter of 0.9525 cm. The inlet of the tube was deployed at 2.5 m above the roof, and was protected by a stainless steel barrel with a diameter of 60 cm. The sampling was controlled with a computer, and the filters were changed automatically. Continuous measurements were performed with a reading frequency of 5 min. The measurement precision and detection limit for black carbon at WO were estimated to be about 5 ng m^{-3} [*Tang et al.*, 1999]. Gaseous HNO_3 and SO_2 were sampled with filter packs, and then analyzed by ion chromatography. The method is the same as

used in CAPMON (the Canadian Air and Precipitation MOnitoring Network). There are three layers of filters in use. The first is Teflon for aerosol sampling without impregnated, the second for HNO_3 sampling as described by *Appel et al.* [1981] and *Shaw et al.* [1982], and the third for SO_2 sampling with K_2CO_3 impregnated. The filter sampling of HNO_3 and SO_2 persisted typically 5 days each time. The detection limit for HNO_3 with this method was estimated to be 1 pptv [*Ma et al.*, 2002, and reference therein].

2.3. Model

[10] A gas-particle equilibrium model EQUISOLV II developed by *Jacobson* [1999b] was used in the present analysis of partitioning between gaseous and particle nitrate at WO. The model applies the Zdanovskii-Stokes-Robinson (ZSR) equation to estimate liquid water content and Bromley's method to estimate mean mixed activity coefficients [*Jacobson et al.*, 1996; *Jacobson*, 1999a, 1999b]. EQUISOLV II can be used to solve equilibrium equations between the gas phase and multiple sizes of the particle phase. It can also be used to solve internal particle equilibrium to provide saturation vapor pressure terms for diffusion-limited mass transfer equations between the gas and multiple sizes of the particle phase. It simulates the H^+-NH_4^+-Na^+-Ca^{2+}-Mg^{2+}-K^+-SO_4^{2-}-NO_3^--Cl^--CO_3^{2-}-H_2O system under both stratospheric and tropospheric conditions. Particle-phase species considered were H_2O(aq), CO_2(aq), and H_2SO_4(aq) as aqueous solvent or solute; NH_4^+(aq), Na^+(aq), Mg^{2+}(aq), Ca^{2+}(aq), K^+(aq), H^+(aq), NO_3^-(aq), Cl^-(aq), HSO_4^-(aq), SO_4^{2-}(aq), Cl^-(aq), HCO_3^-(aq), and CO_3^{2-}(aq) as aqueous solution ions; and NH_4NO_3(s), NH_4Cl(s), NH_4HSO_4(s), $(NH_4)_2SO_4$(s), $(NH_4)_3H(SO_4)_2$(s), NH_4HCO_3(s), $NaNO_3$(s), NaCl(s), $NaHSO_4$(s), Na_2SO_4(s), $NaHCO_3$(s), Na_2CO_3(s), KNO_3(s), KCl(s), $KHSO_4$(s), K_2SO_4(s), $KHCO_3$(s), K_2CO_3(s), $Ca(NO_3)_2$(s), $CaCl_2$(s), $CaSO_4$(s), $CaSO_4$-$2H_2O$(s), $CaCO_3$(s), $Mg(NO_3)_2$(s), $MgCl_2$(s), $MgSO_4$(s), and $MgCO_3$(s) as solid. In addition, formate, acetate and oxalate were considered for the ion balance purpose in the present study.

[11] Gas-phase species considered in the present study were H_2O(g), CO_2(g), and HNO_3(g). Since gaseous NH_3 and HCl were not measured at WO, NH_4^+ and Cl^- in the particle phase were fixed at their observed values for each bin. The particulate species concentrations were initialized with the sampled values for each model bin, the mean diameter of which matched the aerodynamic diameter of the MOUDI. However, large charge imbalances existed in the size bins due to unmeasured ions and/or experimental uncertainties. A charge balance procedure was used to allow the initial sum over all species of charges multiplied by molality to equal zero. This constraint was accomplished by using CO_3^{2-} and H^+ to neutralize the excess positive and negative charges, respectively. In the solving process, nonvolatile species, i.e., Na^+, Ca^{2+}, Mg^{2+}, K^+ and SO_4^{2-}, cannot migrate among the size bins, and thus their predicted size distributions always equal their initial distributions. However, the volatile aerosol species, i.e., H^+, NO_3^- and CO_3^{2-} (excluding NH_4^+ and Cl^- since gas-phase data were not available to initialize these species), may migrate among the various particle size bins via the gas phase until equilibrium has attained.

[12] For each calculation with EQUISOLV II, particles are initialized with some water, regardless of the RH. As such, H^+ can be introduced under all RH conditions where the measurements contained too much net negative charge. As the iteration proceeds under conditions where a solid or multiple solids should be present in equilibrium, the H^+ combines with excess anions (e.g., NO_3^-) to become HNO_3, which evaporates as HNO_3(g), leaving the residual ions to crystallize and the water to dehydrate. In summary, one can add H^+ to balance charge and end up with only solid at the end of the iteration sequence. The same holds true for CO_3^{2-} (which exits as CO_2(g)). When Ca^{2+} is added, it can either form a solid or stay ionized (it will not evaporate). As indicated by *Jacobson* [1999b], no unique solution exists when NH_4NO_3 is simulated to exist in the solid form from NH_3 and HNO_3 when multiple size bins are considered. This situation never occurred in this study, since NH_3 was not solved for (instead, NH_4^+ was constrained to each particle size bin with the measurements).

3. Results and Discussion

[13] A species in the particles can exist in the form of solution ion (e.g., NO_3^-(aq)), liquid (e.g., H_2SO_4(aq)), and solid (e.g., NH_4NO_3(s)). When giving the formula of a species without denoting, e.g., NO_3^-, we are referring to all forms of that species group, i.e., nitrate in aqueous and solid phases.

3.1. Characteristics of Bulk Aerosols

[14] Figure 2 shows the environmental variables and bulk (spectral-integrated over all bins) aerosol group concentrations at WO for each sampling day. It is shown that the aerosol concentrations at WO changed significantly from one day to another, reflecting various air masses associated with different chemical characteristics arriving at WO. Particles at WO are predominantly from natural sources, mainly from soil and crust [*Wen et al.*, 2001; *Gao and Anderson*, 2001], but the perturbations from human sources also exist as indicated by black carbon (BC) concentrations observed at this site [*Tang et al.*, 1999]. *Tang et al.* [1999] reported that the monthly averaged BC concentration at WO varied in the range of 130–300 ng m^{-3} during the period of July 1994 to December 1995. The BC concentration averaged for the period in the present study was 272 ng m^{-3}. Low levels of BC were generally associated with air masses from the west and southwest, which was the predominant wind direction in the fall-winter at WO. High levels of BC at WO were brought in by air masses from the northeast, which could be traced back to the Xining City and other industrial regions upwind [*Tang et al.*, 1999]. Although there was no farming process resulting in large-scale combustion around the site during the season, biomass burning caused occasionally by individual herder's activities could be an alternative source of BC at WO.

[15] Table 1 gives the correlation coefficients (r) among local meteorological parameters, aerosol precursor gases, ionic aerosols, organic aerosols and BC observed at WO. A significant correlation of K^+, NH_4^+ and SO_4^{2-} with BC ($r > 0.9$) indicates that the sources of these aerosols were associated with human activities. This provides further evidence that BC at WO could be attributed to both

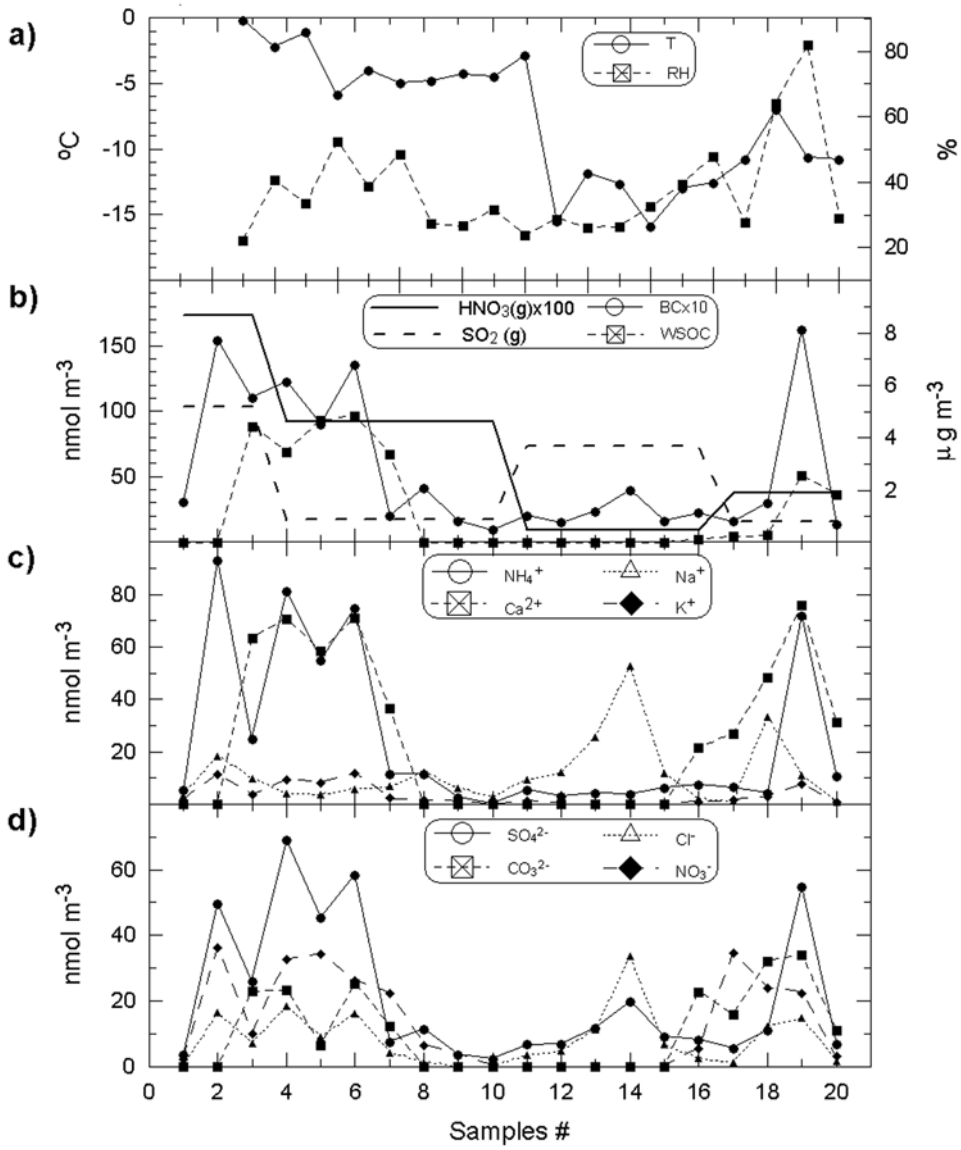

Figure 2. Nighttime averaged (a) temperature, T, and relative humidity, RH, (b) gaseous nitric acid, $HNO_3(g)$, gaseous sulfur dioxide, $SO_2(g)$, water soluble organic carbon, WSOC, and black carbon, BC, (c) bulk particulate cations, and (d) bulk particulate anions for each sample collected at WO. Only weekly averaged data were obtained for $HNO_3(g)$ and $SO_2(g)$. For comparison, the $HNO_3(g)$ and BC plots are amplified by 100 and 10 factors, respectively. The connecting lines do not mean the continuous sampling.

industrial (SO_4^{2-}-related) and biomass burning (K^+-related) sources. There is an anti-correlation between Na^+ with all other aerosol species except Cl^-. High Na^+ values were found only in Sample 14 and 18 (Figure 2), indicating that the sea or lake salt could not be a main source of particles at WO. It appears that the local temperature had little influence on the aerosol concentration, but the effect of relative humidity (RH) was larger. The correlation between RH and aerosol species can be affected by the solubility of volatile species such as CO_2 and water-soluble organic carbon (WSOC), which tend to exist in the particle phase when the aerosol water content is high. It can also be due to the fact that the low RH is typically associated with air masses from the upper troposphere, where the aerosol concentrations are small.

[16] WSOC, Ca^{2+} + CO_3^{2-}, and NH_4^+ + SO_4^{2-} are the three dominant components of the aerosols measured at WO as pointed out by *Li et al.* [2000]. In addition, in this study, a considerable abundance of NO_3^- was found. Table 2 compares the concentrations of gaseous nitric acid, particulate nitrate and total nitrate observed under free tropospheric conditions at the Mauna Loa Observatory (MLO) and WO. The mean particulate NO_3^- concentration was 171 pptv (i.e., 12.3 nmol m^{-3}) at WO. The free tropospheric mean value of particulate NO_3^- at the Mauna Loa Observatory was 30 pptv as reported by *Norton et al.* [1992], but it was 7–13 pptv according to *Galasyn et al.* [1987] for a different period. *Lee et al.* [1994] measured the total nitrate concentration rather than particulate nitrate at MLO. The annual average of total nitrate according to *Lee et al.* [1994] was

Table 1. Correlation Coefficients (r) Among Ion Concentrations and Environmental Variables During the Sampling Period at WO

	T[a]	RH[b]	Na^+	K^+	NH_4^+	Ca^{2+}	Mg^{2+}	Cl^-	NO_3^-	SO_4^{2-}	CO_3^{2-}	OXA	ACE	FOR	WSOC	BC
T[a]	1.00															
RH[b]	−0.08	1.00														
Na^+	−0.36	0.14	1.00													
K^+	0.42	0.54	−0.15	1.00												
NH_4^+	0.33	0.57	−0.13	0.97	1.00											
Ca^{2+}	0.22	0.67	−0.21	0.64	0.60	1.00										
Mg^{2+}	0.24	0.59	−0.23	0.71	0.73	0.89	1.00									
Cl^-	−0.24	0.42	0.73	0.42	0.47	0.27	0.35	1.00								
NO_3^-	0.36	0.47	−0.15	0.79	0.73	0.63	0.58	0.27	1.00							
SO_4^{2-}	0.22	0.62	−0.01	0.92	0.96	0.69	0.84	0.61	0.68	1.00						
CO_3^{2-}	0.00	0.79	−0.10	0.44	0.39	0.87	0.62	0.20	0.51	0.47	1.00					
OXA	0.20	0.67	−0.22	0.75	0.73	0.93	0.94	0.36	0.61	0.84	0.73	1.00				
ACE	0.37	0.28	−0.20	0.57	0.49	0.73	0.75	0.19	0.42	0.58	0.42	0.73	1.00			
FOR	0.30	0.57	−0.18	0.72	0.65	0.92	0.87	0.33	0.56	0.75	0.73	0.95	0.86	1.00		
WSOC	0.36	0.30	−0.30	0.63	0.57	0.86	0.84	0.21	0.52	0.65	0.54	0.84	0.86	0.89	1.00	
BC	0.36	0.62	−0.01	0.91	0.94	0.64	0.72	0.52	0.63	0.93	0.47	0.75	0.60	0.73	0.60	1.00

T, temperature; RH, relative humidity; OXA, oxalate; ACE, acetate; FOR, formate; WSOC, water-soluble organic carbon; and BC, black carbon.

113 pptv. The ground particulate NO_3^- concentration was about 426 pptv at Cheju, Korea [*Carmichael et al.*, 1996, 1997]. The particulate NO_3^- concentration at WO can hence be considered as representative of the free troposphere over continental regions.

[17] As shown in Table 1, there is more significant correlation of particulate NO_3^- with K^+, NH_4^+, Ca^{2+}, Mg^{2+} and BC than with Na^+, implying that nitrate aerosols at WO can be associated with human activities and natural sources other than sea (or lake) salt. This result is different in some aspects from previous studies for marine free tropospheric conditions at MLO. For example, *Norton et al.* [1992] pointed out that the conditions at MLO were not favorable for the existence of ammonium nitrate, and sodium was one of the most readily available cations which could assist in forming an aerosol nitrate salt. However, an anti-correlation of particulate NO_3^- with Na^+ was found for WO (Table 1). On the other hand, agreements exist between the two sites, e.g., particulate nitrate having been influenced by mineral calcite at both sites. As discussed in the paper of *Norton et al.* [1992], high nitrate at MLO might be associated with nitric acid deposition on Asian dust. According to *Lee et al.* [1994], springtime peak total nitrate corresponded to incidents of increased Asian dust over the northern Pacific Ocean, and summer high total nitrate resulted from the long-range transport from the North American continent. Although nitric acid is very volatile, it is also highly soluble in water and has a large tendency to adsorb on surfaces. It is possible that black carbon and dust particles adsorb nitric acid vapor effectively, retaining it in the aerosol phase.

[18] In contrast to the situation of particulate nitrate, gaseous nitric acid at WO was 3–10 times lower at WO than at MLO (Table 2). Free tropospheric particulate nitrate against nitric acid showed a negative correlation at MLO [*Norton et al.*, 1992]. Although there was no daily measurement of HNO_3 at WO, HNO_3 appeared to be correlated with particulate NO_3^- (Figure 2). At MLO the majority of nitrate was usually in the gas phase, while at WO nitrate existed mainly in the particle phase during the observation period. This difference can be due to the different capability for sea-salt and dust particles to adsorb nitric acid vapor. It can also be due to various environmental conditions such as temperature and relative humidity, which affect the equilibration of volatile species between the gas and particle phases as well. One should note that the field experiments mentioned above were carried out in different seasons, with the spring-summer periods at MLO [*Norton et al.*, 1992; *Galasyn et al.*, 1987] and a fall-winter period at WO (this study), respectively.

3.2. Size Distribution of Ionic Aerosols

[19] The size distributions of the following species, Ca^{2+}, CO_3^{2-}, NH_4^+, SO_4^{2-}, Na^+, Cl^- and WSOC, have been published previously by *Li et al.* [2000]. However, the nitrate, oxalate and potassium data, which were collected as part of the same experiment, were not published. Of the total 20 samples, four (Samples 2, 3, 5 and 7) were selected for analysis in the present study. The rest were not taken into account due to either the negligible amount of NO_3^- (Samples 1, 8–16 and 20), detection values occurring in some bins (Samples 4, 6 and 19), or because the NO_3^- distribution replicated that in Sample 7 (Samples 17 and 18).

[20] Figure 3 shows the size distribution of aerosol species as a function of aerodynamic diameter (d_{50}) at WO for each case of the four samples. In all the cases, NH_4^+, SO_4^{2-}, K^+ and $C_2O_4^{2-}$ (oxalate ions) accumulate in the fine mode ($D_p < 2.0$ μm), and Ca^{2+} (with CO_3^{2-}, not shown) accumulate in the coarse mode. Na^+ and Cl^- exist either in the coarse mode (Cases 2 and 4) or in the transition region between the fine and coarse modes (Cases 1 and 3). The size distribution of NO_3^- is quite different from one case

Table 2. Comparison of Free Tropospheric Gaseous Nitric Acid (HNO_3), Particulate Nitrate (p-NO_3^-) and Total Nitrate (t-nitrate) Observed at MLO and WO

HNO_3, pptv	p-NO_3^-, pptv	t-nitrate, pptv	Source	Reference
15–23	7–13		MLO, April–June	*Galasyn et al.* [1987]
103	30		MLO, May–June	*Norton et al.* [1992]
		113	MLO, Annual	*Lee et al.* [1994]
9.5	171		WO, Nov.–Jan.	This study

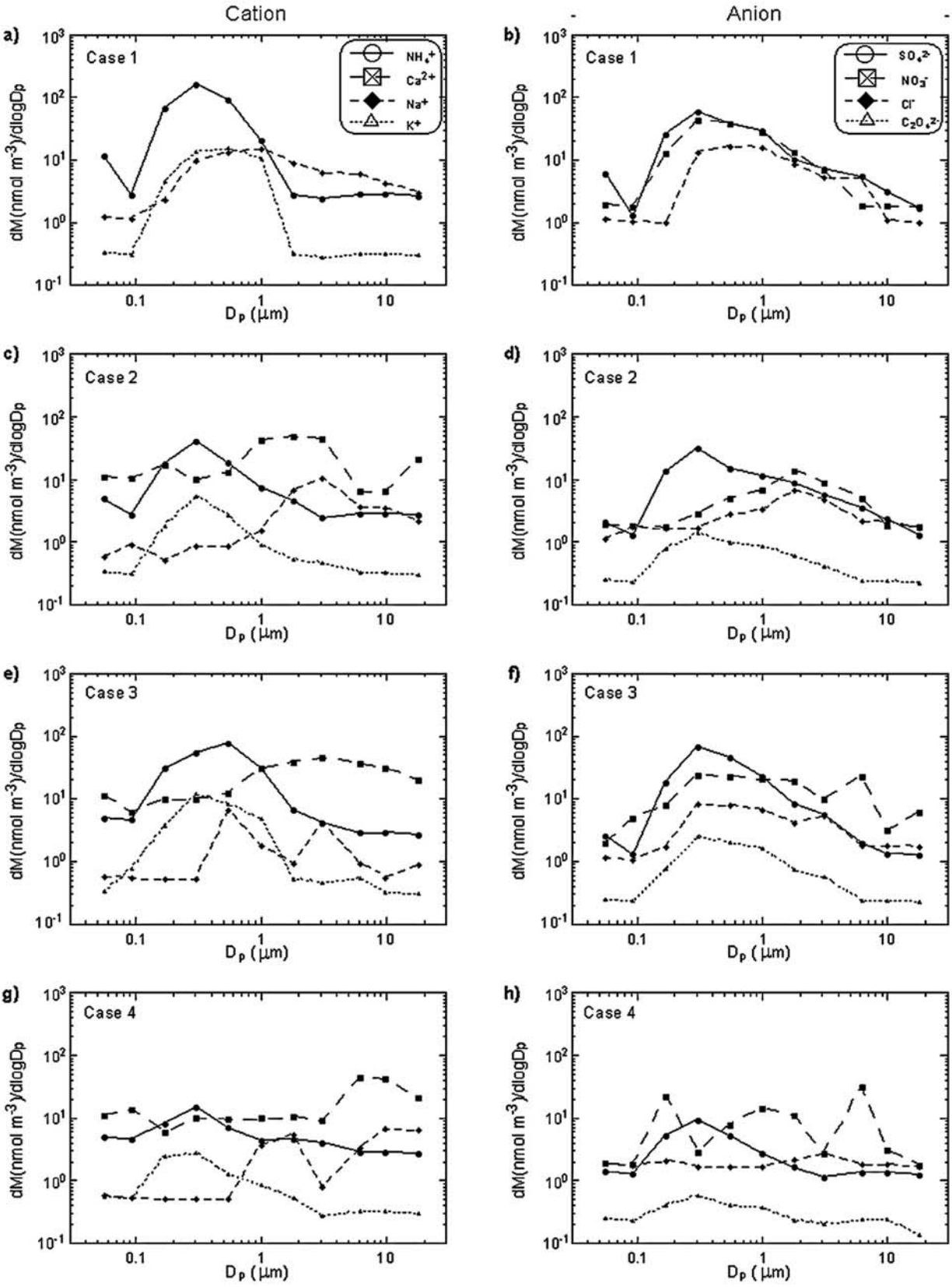

Figure 3. Size distributions of ionic aerosols as a function of aerodynamic diameter in the 4-selected cases at WO. Cations are shown in the left panels, and anions in the right ones. Calcium and oxalate are not presented in Case 1 where their levels were below the detection limits.

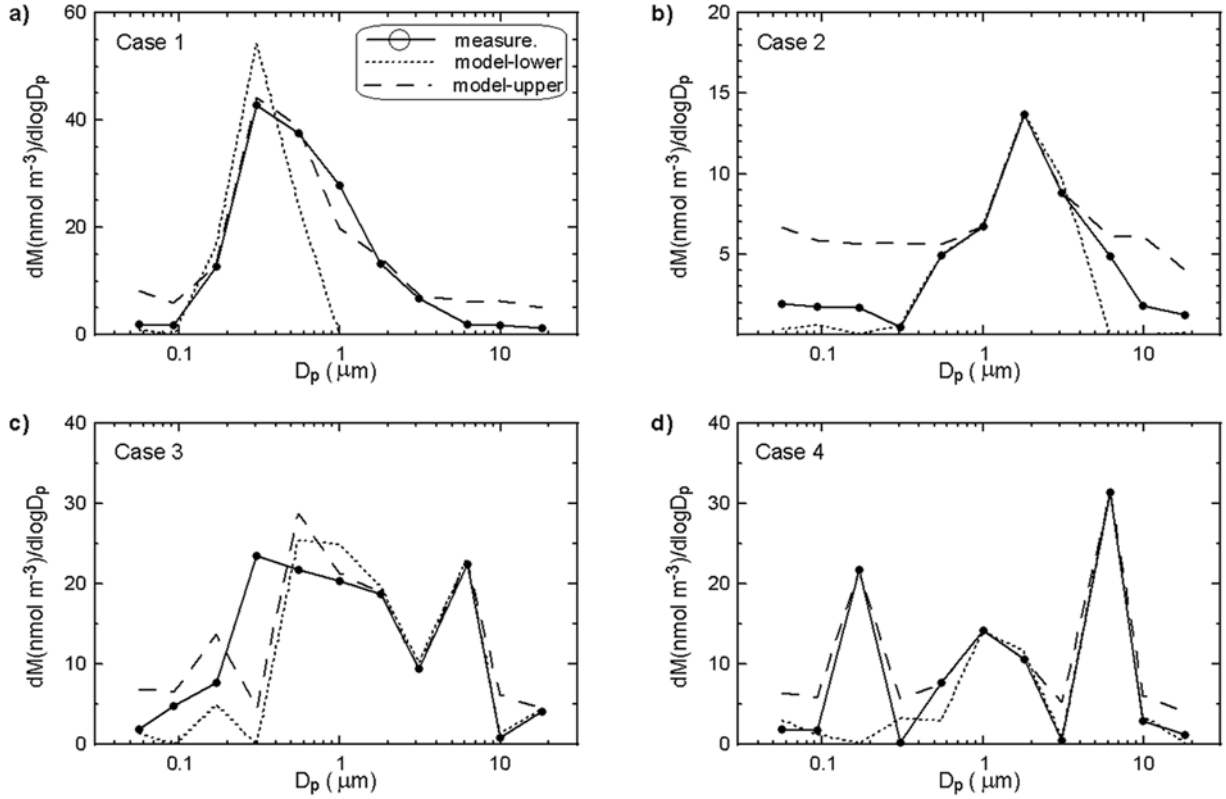

Figure 4. Size distributions of observed (solid lines with circles) and simulated (dashed lines and dotted lines) particulate NO_3^- in the 4-selected cases at WO. Dashed lines and dotted lines refer to model simulations initialized with (model-high) and without (model-low) setting the detection limits for small ionic aerosol concentrations.

to another. NO_3^- accumulates in the fine mode for Case 1, in the coarse mode for Case 2 and in both the fine and coarse modes for Case 3. For case 4 there is an abnormal size distribution of NO_3^- with three peaks occurring in and between the fine and coarse modes.

[21] The size distribution pattern of NO_3^- observed at WO is different from that in previous studies at some marine sites in East Asia, where nitrate exists exclusively in the coarse mode [e.g., *Nishikawa et al.*, 1991; *Carmichael et al.*, 1996]. It should be noted that those Korean or Japanese sites are located in the Far East Asia, in the downstream regions of long-range transport of continental dust and pollution. Therefore aging has favored the accumulation of NO_3^- in the coarse mode before air masses arrived at those sites [*Song and Carmichael*, 1999, 2001b]. The observed particulate-to-total nitrate ratio (total nitrate = particulate nitrate + gaseous nitric acid) was 0.95, 0.88, 0.97 and 0.96 for Cases 1–4, respectively. These values are much larger than the one of ~0.3 for the remote troposphere over the Pacific [*Song and Carmichael*, 2001a, and references therein]. The observed fine-to-global particulate nitrate ratio was 0.92, 0.65, 0.73 and 0.62 for Cases 1–4, respectively (with $D_p < 2.0$ μm for the fine mode). This suggests that the amount of NO_3^- residing in the fine mode is more than or comparable with that in the coarse mode at WO. *Ayers et al.* [1997] showed that acidity and surface area of particles in different size have a large impact on the size distribution of condensing species like oxalic acid in the aerosol phase. Below we will examine the size-distributed chemistry related to particulate nitrate at WO further.

3.3. Equilibration of Particulate Nitrate With Gaseous Nitric Acid

[22] As described in section 2.3 above, we used EQUISOLV II to analyze the partitioning between gaseous and particle nitrate at WO. The volatile species concentrations were either initialized with gas- and particle-phase measurements (HNO_3 and NO_3^-) or constrained to their observed values in each size bin (NH_4^+ and Cl^-). CO_2 is solved between the gas and particle phases when $CO_2/H_2CO_3/HCO_3^-/CO_3^{2-}$ are turned on, and H_2O is not used unless it is turned on as active species (only RH is used). Therefore predicted size distributions of particulate nitrate with the model should theoretically be the same as the measurements with which they were initialized if equilibrium existed between gaseous nitric acid and particulate nitrate. However, deviations between the predicted and measured size distributions of particulate nitrate do exit for various reasons [*Fridlind and Jacobson*, 2001]. The general sources of error include (1) error in the model assumptions (e.g., lack of actual equilibrium between the gas and particle phases), (2) error in the model calculations (e.g., error in the estimated water uptake slats), or (3) error in the estimated or measured concentrations of gases or aerosols (e.g., experimental uncertainty in measured Ca^{2+} concentration).

[23] Figure 4 presents the observed and simulated size distribution of particulate NO_3^- as a function of aerodynamic

diameter for each selected sample at WO. For each case, two model simulations were performed with two sets of different initial ionic aerosol concentrations, respectively. We set zero as the minimum values of initial ionic aerosol concentrations for one simulation, and for another simulation we set the detection limits as the minimum values of those concentrations. The detection limits of some ions have been given in section 2.2 above. As shown in the figure, the NO_3^- size distribution was generally reproduced by the model within the uncertainty ranges caused by the detection limits of aerosols in the measurements. An exception exists for Bin 4 (D_p = 0.3 μm) in Case 3, where the accumulation-mode NO_3^- was significantly underestimated with respect to the measurements. The reason for this may be missing cations (e.g., NH_4^+, Na^+, K^+, Mg^{2+} or Ca^{2+}) measured in the bin. In addition to carrying out the above simulations, we also carried out simulations for all the four cases with a different initial charge-balance treatment. We added Ca^{2+} (instead of H^+) to all the net negative charge bins without setting the detection limits as the minimum values for ionic aerosol concentrations. The NO_3^- results were nearly perfect across the distribution (not shown), suggesting that some cations might not be accounted for, or NO_3^- itself might not be well-measured in some bins.

[24] Nitrate gas-to-particle transfer processes involve acidic nitric acid and this volatile species tends to condense in the more alkaline regions of the aerosol size distribution. Effects of acidity of aerosol particles on the gas-to-particle transfer of nitric acid or its similar condensing species like oxalic acid were investigated for the conditions of marine free troposphere, marine boundary layer and ground continental rural area [*Norton et al.*, 1992; *Ayers et al.*, 1997; *Lefer and Talbot*, 2001]. Acidity of a particle is determined to a large extent by its ionic composition [*Fridlind and Jacobson*, 2000; *Kerminen et al.*, 2001]. Theoretically, there should be a balance between the cations and anions for each size-resolved aerosol sample. However, imbalance in ions used to occur due to errors from the sampling and analysis processes, or due to failures in detecting some chemical compositions. An unbalanced ion balance can be used to provide information about the chemistry of the aerosol [*Kerminen et al.*, 2001]. For example, a cation-to-anion ratio significantly greater than one indicates the presence of soluble organic anions that have not been detected. On the other hand, a cation-to-anion ratio clearly below unity indicates that the particle is quite acidic [*Kerminen et al.*, 2001].

[25] As described in section 2.2, there were detection limits for each ion in the experiment of this study, with the detection limit of Ca^{2+} being one order higher than those of others. The uncertainties caused by these detection limits, of Ca^{2+} in particular, can affect the estimation of the ion balance and acidity significantly, leading to uncertainties in the predicted size distribution of particulate NO_3^-. Ion imbalance was found to exist in each sample at WO and herewith we just take Case 1 in illustration of this effect. Figure 5 shows the ion imbalance, expressed with cation fraction, and model-predicted pH and water content as a function of particle size for Case 1 at WO. The fraction was calculated with two sets of different initial ionic aerosol concentrations. For one set we used the zero value as the minimum concentrations, and for another set we used the

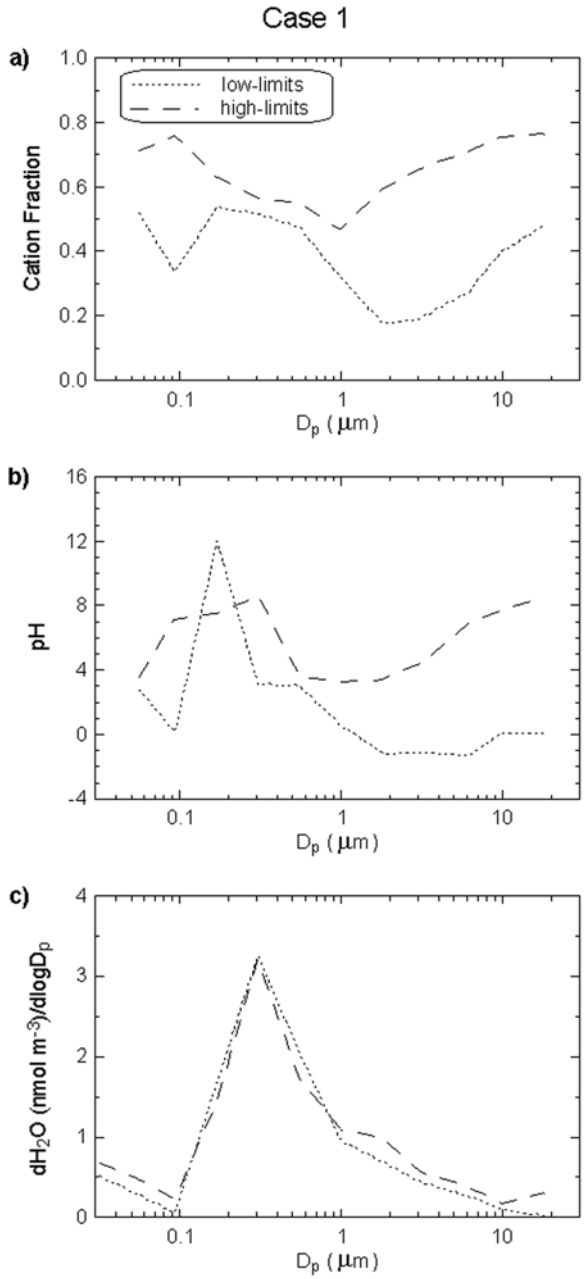

Figure 5. Size distributions of (a) cation fraction, expressed as the total equivalent amount of cations divided by the total equivalent amount of ions, and (b) model-predicted pH and (c) water content for Case 1. Dashed lines and dotted lines refer to values derived with (high-limits) and without (low-limits) setting the detection limits for small ionic aerosol concentrations. There existed ion imbalance in both low- and high-limit cases of Figure 5a. Charge was exactly balanced with H^+ or CO_3^{2-} for the pH prediction in both cases of Figure 5b and Ca^{2+}, Mg^{2+}, and K^+ were neglected and all other components except NO_3^- were constrained to the particle phase in the low-limit case. The low-limit case might be "unrealistic" in the coarse mode as indicated by the too low pH (Figure 5b) and large disagreements between measured and simulated NO_3^-s (Figure 4a), suggesting that additional cations (e.g., Ca^{2+}, Mg^{2+}, and/or K^+) should be present in this mode.

detection limits as the minimum concentrations. While a cation fraction of 0.5 refers to an ion balance, a fraction higher or lower than 0.5 stands for a cation rich or deficient case, respectively. The most prominent effect due to uncertainties in measurements was found in the mode of $D_p \geq 1.0$ μm. The uncertainties in ionic concentrations, mainly from Ca^{2+}, affect the ion balance significantly, from the cation deficient of the low-Ca^{2+} case to the cation rich of the high-Ca^{2+} case (Figure 5a). Charge was exactly balanced with H^+ or CO_3^{2-} for the pH prediction in both cases of Figure 5b and Ca^{2+}, Mg^{2+}, and K^+ were neglected and all other components except NO_3^- were constrained to the particle phase in the low-limit case. Acidity of aerosol particles also changes from the strong acid of the low-Ca^{2+} case to the weak acid or basic of the high-Ca^{2+} case (Figure 5b). As a result, the predicted size distribution of particulate NO_3^- varies significantly in the coarse mode (Figure 4a). The low-limit case might be "unrealistic" in the coarse mode as indicated by too low pH (Figure 5b) and large disagreements between measured and simulated NO_3^- (Figure 4a). Figure 5c shows that the size distribution of water content is determined predominantly by the total molarity in each size bin (Figures 3a–3b). The influence of pH on the water content is negligent, or the vice versa, is negligent in this case.

3.4. Chemical Pathways for the Formation of Particulate Nitrate

[26] The process that results in the generation of fine nitrate particles is the reaction of gaseous nitric acid with gaseous ammonia,

$$NH_3(g) + HNO_3(g) \rightarrow NH_4NO_3(a) \quad \text{(R1)}$$

The reactions in which HNO_3 replaces water-soluble particulate formate, acetate and oxalate, e.g.,

$$(NH_4)_2C_2O_4(a) + 2HNO_3(g) \rightarrow 2NH_4NO_3(a) + C_2H_2O_4(g) \quad \text{(R2)}$$

are also an important formation pathway for fine nitrate particles [*Tabazadeh et al.*, 1998]. The organic anions can be abundant in fine particles, such as those from biomass burning [*Talbot et al.*, 1988; *Andreae et al.*, 1988]. On the other hand, coarse nitrate particles can be produced by the reaction of gaseous nitric acid with mineral aerosols,

$$CaCO_3(a) + 2HNO_3(g) \rightarrow Ca(NO_3)_2(a) + H_2O + CO_2(g) \quad \text{(R3)}$$

and with sea (or lake) salt aerosols,

$$NaCl(a) + HNO_3(g) \rightarrow NaNO_3(a) + HCl(g) \quad \text{(R4)}$$

[27] Aerosol NH_4^+ is always correlated with SO_4^{2-} (Table 1), and tends to coexist more easily with SO_4^{2-} than with NO_3^- in the particle phase. The reaction (R1) is important only when NH_4^+ is excessive in comparison with SO_4^{2-} in the particles. Therefore we use NH_4^+-$2SO_4^{2-}$ to represent a potential of NO_3^- forming via (R1). Since we cannot distinguish the biomass burning related NH_4^+ from other sources of NH_4^+, we use K^+-$2C_2O_4^{2-}$, instead of NH_4^+-$2C_2O_4^{2-}$, to represent a signature of NO_3^- forming via (R2). Large fraction of potassium in the fine particles associated with biomass burning was also observed during the Indian Ocean Experiment (INDOEX) [*Lelieveld et al.*, 2001]. Similarly, $2Ca^{2+}$-$2CO_3^{2-}$ and Na^+-Cl^- are used as an indicator of NO_3^- sources via (R3) and (R4), respectively. Figure 6 shows the size distributions of the difference NH_4^+-$2SO_4^{2-}$, $2Ca^{2+}$-$2CO_3^{2-}$, Na^+-Cl^- and K^+-$2C_2O_4^{2-}$ in the 4-selected cases. For Case 1, the accumulation of NO_3^- in the fine mode of $D_p < 1.0$ μm (Figure 4) can be attributed mainly to the reaction (R1) as indicated by the positive peak of NH_4^+-$2SO_4^{2-}$. The possibility of NO_3^- forming via reaction (R1) is much less in the other cases (Cases 2–4), where nearly all NH_4^+ can exist exclusively in the form of $(NH_4)_2SO_4$ or NH_4HSO_4. The accumulation of NO_3^- in the fine mode can also be attributed, to a less extent, to the reaction (R2) as indicated by the distribution of K^+-$2C_2O_4^{2-}$, for Case 1 in particular. For Cases 2–4, the reaction (R3) plays a dominant role in the accumulation of NO_3^- in the coarse mode as demonstrated by the distribution of $2Ca^{2+}$-$2CO_3^{2-}$. The underestimation of NO_3^- at $D_p = 0.3$ μm (Bin 4) of Case 3 as pointed out above can be attributed to the negative peak of NH_4^+-$2SO_4^{2-}$ that are caused most possibly by a great amount of NH_4^+ not accounted in that bin. Since we used the ionic aerosol concentrations for Figure 6 without setting the minimum values using the detection limits, the NO_3^- peak at $D_p = 0.09$ μm (Bin 3) of Case 4 was not reproduced (Figure 4) and traced by any ions difference (Figure 6). The reaction (R4) is not important at WO as indicated by the distribution of Na^+-Cl^- in Figure 6.

4. Conclusions

[28] We presented the size distributions of particulate nitrate, NO_3^-, along with other aerosols measured during the fall-winter periods at Waliguan Observatory (WO) on the Tibetan Plateau. The mean particulate NO_3^- concentration was 171 pptv (12.3 nmol m^{-3}) at WO, representing a background condition of the continental free troposphere. We found that the size distribution of NO_3^- was quite different from one sample to another. NO_3^- accumulated either in the fine mode, in the coarse mode, or in both the fine and coarse modes. In some samples three peaks of NO_3^- were found across the distribution. The size distribution of NO_3^- was reasonably reproduced with the gas-particle equilibrium model EQUISOLV II when the uncertainties caused by the detection limits of aerosols were considered, but some differences might also be due to nonequilibrium in some cases.

[29] We found that nitrate at WO existed mainly in the particle phase. The observed particulate-to-total nitrate ratio (total nitrate = particulate nitrate + gaseous nitric acid) was about 0.9 at WO, much larger than the values obtained for the remote troposphere over the Pacific. Our measurements showed that particulate nitrate in the fine mode ($D_p < 2.0$ μm) was higher than or comparable with that in the coarse mode at WO. This finding disagrees with previous studies in the remote troposphere over the western Pacific, where a relatively large fraction of sulfate and nitrate exit in the coarse mode [*Carmichael et al.*, 1996; *Dentener et al.*, 1996; *Song and Carmichael*, 2001a, 2001b]. Our analyses

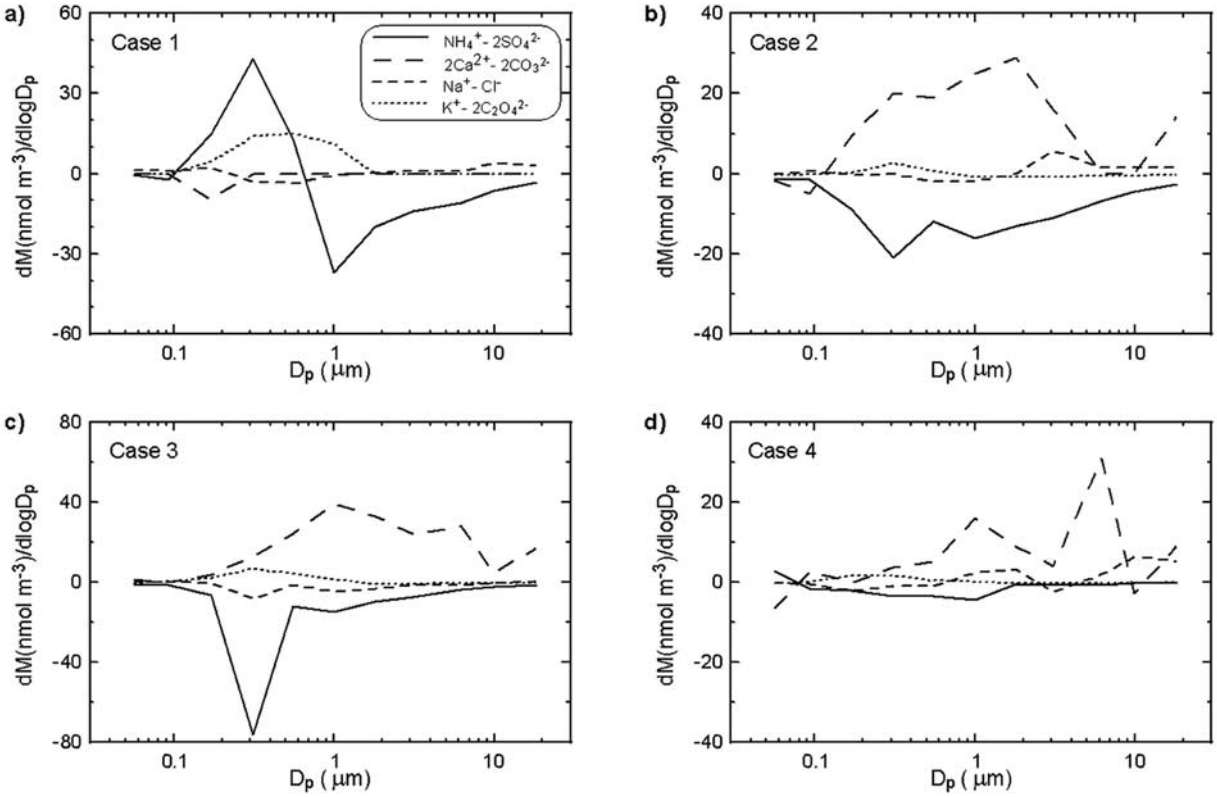

Figure 6. Size distributions of the difference NH_4^+-$2SO_4^{2-}$ (solid lines), $2Ca^{2+}$-$2CO_3^{2-}$ (long dashed lines), Na^+-Cl^- (short dashed lines) and K^+-$2C_2O_4^{2-}$ (dotted lines) in the 4-selected cases at WO. The concentrations of CO_3^{2-} were from the model simulations, while those of other ionic aerosols were from the measurements.

indicated that fine nitrate particles at WO were produced most likely by the reaction of gaseous nitric acid with gaseous ammonia, while coarse nitrate particles at WO were generated via the condensing of nitric acid on the surface of mineral aerosols. Our measurements of black carbon at WO indicated that air masses perturbed by human activities arrived at this background site frequently. In addition to the long-range transport of sulfate, which is originally from fuel combustion, the signature of biomass burning at WO was found to be associated with black carbon as well as the accumulation of potassium and oxalate in the fine particles.

[30] **Acknowledgments.** This work was under the auspices of the China National Key Project for Basic Research (G1999045700). MZJ was supported by the NASA Atmospheric Chemistry and Analysis Program, the Environmental Protection Agency Office of Air Quality Planning and Standards, and the National Science Foundation Atmospheric Chemistry Division. We are greatly indebted to Husheng Xue and all the staff at the Waliguan Observatory for their support during the field experiment. We would like to thank the two anonymous reviewers for their helpful comments on the manuscript.

References

Andreae, M., et al., Biomass-burning emissions and associated haze layers over Amazonia, *J. Geophys. Res.*, *93*, 1509–1527, 1988.

Appel, B. R., Y. Tokiwa, and M. Haik, Sampling of nitrate in ambient, *Atmos. Environ.*, *15*, 283–289, 1981.

Ayers, G. P., J. M. Cainey, R. W. Gilett, and J. P. Ivey, Atmospheric sulphur and cloud condensation nuclei in marine air in the Southern Hemisphere, *Philos. Trans. R. Soc. London Ser. B*, *352*, 203–211, 1997.

Carmichael, G. R., Y. Zhang, L.-L. Chen, M.-S. Hong, and H. Ueda, Seasonal variation of aerosol composition at Cheju Island, Korea, *Atmos. Environ.*, *30*, 2407–2416, 1996.

Carmichael, G. R., et al., Aerosol composition at Cheju Island, Korea, *J. Geophys. Res.*, *102*, 6010–6047, 1997.

Chen, L. L., et al., Influence of continental outflow events on the aerosol composition at Cheju Island, Korea, *J. Geophys. Res.*, *102*, 28,551–28,573, 1997.

Dentener, F. J., and P. J. Crutzen, Reaction of N_2O_5 on tropospheric aerosols: Impact on the global distributions of NO_x, O_3, and OH, *J. Geophys. Res.*, *98*, 7149–7163, 1993.

Dentener, F. J., G. R. Carmichael, Y. Zhang, J. Lelieveld, and P. J. Crutzen, Role of mineral aerosol as a reactive surface in the global troposphere, *J. Geophys. Res.*, *101*, 22,869–22,889, 1996.

Ehhalt, D. H., and J. W. Drummond, The troposphere cycle of NO_x, in *Chemistry of the Unpolluted and Polluted Troposphere*, edited by H. W. Georgii and W. Jaeschke, pp. 219–251, D. Reidel, Norwell, Mass., 1982.

Fridlind, A. M., and M. Z. Jacobson, A study of gas-aerosol equilibrium and aerosol pH in the remote marine boundary during the First Aerosol Characterization Experiment (ACE 1), *J. Geophys. Res.*, *105*, 17,325–17,340, 2001.

Galasyn, J. F., K. L. Tschudy, and B. J. Huebert, Seasonal and diurnal variability of nitric acid vapor and ionic aerosol species in the remote free troposphere at Mauna Loa, Hawaii, *J. Geophys. Res.*, *92*, 3105–3133, 1987.

Gao, Y., and J. R. Anderson, Characteristics of Chinese aerosols determined by individual-particle analysis, *J. Geophys. Res.*, *106*, 18,037–18,045, 2001.

Gard, E. E., et al., Direct observation of heterogeneous chemistry in the atmosphere, *Science*, *279*, 1184–1187, 1998.

Hansen, A. D. A., H. Rosen, and T. Novokov, The aethalomete-ran instrument for the real time measurement of optical absorption by aerosol particles, *Sci. Total Environ.*, *36*, 191–196, 1984.

Jacobson, M. Z., *Fundamentals of Atmospheric Modeling*, 656 pp., Cambridge Univ. Press, New York, 1999a.

Jacobson, M. Z., Studying the effects of calcium and magnesium on size-distributed nitrate and ammonium with EQUISOLV II, *Atmos. Environ.*, *33*, 3635–3649, 1999b.

Jacobson, M. Z., A. Tabazadeh, and R. P. Turco, Simulating equilibrium within aerosols and nonequilibrium between gases and aerosols, *J. Geophys. Res.*, *101*, 9079–9091, 1996.

Kerminen, V.-M., R. Hillamo, K. Teinilä, T. Pakkanen, I. Allegrini, and R. Sparapani, Ion balances of size-resolved tropospheric aerosol samples: Implications for the acidity and atmospheric processing of aerosols, *Atmos. Environ.*, *35*, 5255–5265, 2001.

Lee, G., J. T. Merrill, and B. Huebert, Variation of free tropospheric total nitrate at Mauna Loa Observatory, Hawaii, *J. Geophys. Res.*, *99*, 12,821–12,831, 1994.

Lefer, B. L., and R. W. Talbot, Summertime measurements of aerosol nitrate and ammonium at a northeastern U.S. site, *J. Geophys. Res.*, *106*, 20,365–20,378, 2001.

Lelieveld, J., et al., The Indian Ocean Experiment: Widespread air pollution form South and Southeast Asia, *Science*, *291*, 1031–1036, 2001.

Li, S.-M., J. Tang, H. S. Xue, and D. Toom-Sauntry, Size distribution and estimated optical properties of carbonate, water-soluble organic carbon and sulfate in aerosols at a remote high altitude site in western China, *Geophys. Res. Lett.*, *27*, 1107–1110, 2000.

Ma, J., J. Tang, X. J. Zhou, and X. S. Zhang, Estimates of the chemical budget for ozone at Waliguan Observatory, *J. Atmos. Chem.*, *41*, 21–48, 2002.

Marple, V. A., K. L. Rubow, and S. M. Behm, A Microorifice Uniform Deposit Impactor (MOUDI): Description, calibration, and use, *Aerosol Sci. Techol.*, *14*, 434–446, 1991.

Moya, M., A. S. Ansari, and S. N. Pandis, Partitioning of nitrate and ammonium between the gas and particulate phase during the 1997 IMADA-AVER study in Mexico City, *Atmos. Environ.*, *35*, 1791–1804, 2001.

Nishikawa, M., S. Kanamori, N. Kanamori, and T. Misoguchi, Kosa aerosols as eolian carrier of anthropogenic material, *Sci. Total Environ.*, *107*, 13–27, 1991.

Norton, R. B., et al., Measurements of nitric acid and aerosol nitrate at the Mauna Loa Observatory during the Mauna Loa Observatory Photochemistry Experiment 1988, *J. Geophys. Res.*, *97*, 10,415–10,425, 1992.

Perry, K. D., T. A. Cahill, R. C. Schnell, and J. M. Hurris, Long-range transport of anthropogenic aerosols to the National Oceanic and Atmospheric Administration baseline station at Mauna Loa Observatory, Hawaii, *J. Geophys. Res.*, *104*, 18,521–18,533, 1999.

Prospero, J. M., and D. L. Savoie, Effects of continental sources on nitrate concentrations over the Pacific Ocean, *Nature*, *339*, 687–689, 1989.

Rosen, H., A. D. A. Hansen, L. Gundel, and T. Novokov, Identification of the optically absorbing component in urban aerosols, *Nappl. Opt.*, *17*, 3859–3861, 1978.

Savoie, D. L., and J. M. Prospero, Particle size distribution of nitrate and sulfate in the marine atmosphere, *Geophys. Res. Lett.*, *9*, 1207–1210, 1982.

Savoie, D. L., and J. M. Prospero, Comparison of oceanic and continental sources of non-sea-salt sulfate over the Pacific Ocean, *Nature*, *339*, 685–687, 1989.

Sempere, R., and K. Kawamura, Low molecular weight dicarboxylic acids and related polar compounds in the remote marine rain samples collected from western Pacific, *Atmos. Environ.*, *30*, 1609–1619, 1996.

Shaw, R. W., Jr., R. K. Stevens, and J. Bowermaster, Measurements of atmospheric nitrate and nitric acid: The denuder difference method, *Atmos. Environ.*, *16*, 845–853, 1982.

Song, C. H., and G. R. Carmichael, The aging process of naturally emitted aerosol (sea-salt and mineral aerosol) during long range transport, *Atmos. Environ.*, *33*, 2203–2218, 1999.

Song, C. H., and G. R. Carmichael, Gas-particle partitioning of nitric acid modulated by alkaline aerosol, *J. Atmos. Chem.*, *40*, 1–22, 2001a.

Song, C. H., and G. R. Carmichael, A three-dimensional modeling investigation of the evolution processes of dust and sea-salt particles in east Asia, *J. Geophys. Res.*, *106*, 18,131–18,154, 2001b.

Stelson, A. W., and J. H. Seindeld, Relative humidity and pH dependence of the vapor pressure of ammonium nitrate-nitric acid solutions, *Atmos. Environ.*, *16*, 993–1000, 1982.

Stelson, A. W., S. K. Friedlander, and J. H. Seindeld, A note on the equilibrium relationship between ammonia and nitric acid and particulate ammonium nitrate, *Atmos. Environ.*, *13*, 369–371, 1979.

Tabazadeh, A., M. Z. Jacobson, H. B. Singh, O. B. Toon, J. S. Lin, R. B. Chatfield, A. N. Thakur, R. W. Talbot, and J. E. Dibb, Nitric acid scavenging by mineral and biomass burning aerosols, *Geophys. Res. Lett.*, *25*, 4185–4188, 1998.

Talbot, R. W., M. O. Andreae, T. W. Andreae, and R. C. Harriss, Regional aerosol chemistry of the Amazon basin during the dry season, *J. Geophys. Res.*, *93*, 1499–1508, 1988.

Tang, J., Y. P. Wen, X. B. Xu, X. D. Zheng, S. Guo, and Y. C. Zhao, China Global Atmosphere Watch Baseline Observatory and its measurement program, in *CAMS Annual Report 1994–1995*, pp. 56–65, China Meteorol. Press, Beijing, 1995.

Tang, J., Y. P. Wen, L. X. Zhou, D. L. Qi, M. Zheng, N. Trivett, and E. Wallgren, The observational study of black carbon in clean air area of western China, *Q. J. Appl. Meteorol.*, *10*, 160–170, 1999.

Wen, Y. P., X. B. Xu, J. Tang, Y. C. Zhao, and X. C. Zhang, Enrichment characteristics and origin of atmospheric aerosol elements at Mt. Waliguan, *Q. J. Appl. Meteorol.*, *12*, 400–408, 2001.

M. Z. Jacobson, Department of Civil & Environmental Engineering, Terman Engineering Center, Room M-13, Stanford University, Stanford, CA 94305, USA. (jacobson@ce.stanford.edu)

S.-M. Li, Atmospheric Environment Service, 4905 Dufferin Street, Downsview Ontario M3H 5T4, Canada. (shao-meng.li@ec.gc.ca)

J. Ma and J. Tang, Chinese Academy of Meteorological Sciences, 46 Zhong-Guan-Cun Nan-Da-Jie Beijing 100081, China. (maj@public.bta.net.cn; tangj@cams.cma.gov.cn)